MICROCOPY RESOLUTION TEST CHART
NATIONAL BUREAU OF STANDARDS 1963 A

-1-

AN ADAPTIVE, NOISE TOLERANT, FREQUENCY EXTRAPOLATION ALGORITHM
FOR DIFFRACTION CORRECTED ULTRASOUND TOMOGRAPHY

F. Stenger[1,2]*
M. J. Berggren[2]†
S. A. Johnson[2]†
Y. Li[2]

*Department of Mathematics
†Department of Bioengineering
University of Utah
Salt Lake City, Utah 84112

Abstract

In our previous work [1], a procedure was developed, based on algorithms for rational function frequency extrapolation and L_1-norm averaging to circumvent both the effects of noise, and errors due to refracted curved paths, for solving the inverse scattering problem in ultrasonic imaging. In this paper, we reverse the order of the first two algorithms with respect to [1]; that is, we first apply the L_1 averaging procedure and then carry out the rational function procedure, extrapolating to infinite frequency. An adaptive method for choosing the best rational function expansion is also employed. We describe the underlying ideas of the procedure, and we illustrate examples of reconstructions in the presence and absence of Gaussian noise. These results are then compared with results of previous experiments. The resulting procedure works with a much smaller signal-to-noise ratio. An extension is suggested to image speed of sound and density.

1. Mathematical Basis for the Algorithms

1.1 The Physical Problem

Let us assume that sound at high frequency penetrates a body B immersed in fluid. We denote the spatial sound pressure and the corresponding sound source by u and u^i, respectively. The velocity of sound in the fluid is given by c_o, and the velocity of sound in the body by $c(\bar{r})$. A particular path along which sound travels from a source point $\bar{r}_s$ to a detector point $\bar{r}_d$ is denoted by L if it is a straight line path and by P if it is a curved path.

1.2 Differential Equations and Their Asymptotic Solutions

Several derivations exist in the literature of partial differential equations which govern the way sound travels through B. For example, the Helmholtz equation model is given by

$$\nabla^2 u + k^2 u = -k^2 fu \qquad (1.1)$$

where

$$f(\bar{r}) = \frac{c_o^2}{c^2(\bar{r})} - 1, \quad k = \frac{\omega}{c_o} . \qquad (1.2)$$

The Ricatti model,

$$\nabla^2 w + \nabla w \cdot \nabla w + \frac{2 \nabla u_i}{u_i} \cdot \nabla w = -k^2 f \qquad (1.3)$$

is obtained from (1.1) by applying the transform

$$u(\bar{r}) = u_i(\bar{r}) \exp (w) \qquad (1.4)$$

The Rytov model is obtained from (1.3) by dropping the term containing $\nabla w \cdot \nabla w$.

A differential equation governing the flow of sound through B may depend on other properties of B, such as the density $\rho(\bar{r})$ and the compressibility $\kappa(\bar{r})$. In general, such an equation may take the form

$$Au + F(\bar{r}, \rho(\bar{r}), \kappa(\bar{r}), u, k) = 0 \qquad (1.5)$$

where A is a differential operator.

The success of the asymptotic procedure depends on our knowing an asymptotic expression for some function $\phi(u, k)$ which we can compute or measure for a range of values of k. For example, $\phi(u, k)$ may have the asymptotic expression

$$\phi(u, k) = a(k)[v(\kappa, \rho) + \epsilon(k, \kappa, \rho)] \qquad (1.6)$$

83

where $a(k)$ is a known function,

$$\varepsilon(k, \kappa, \rho) = O(k^{-\sigma}) \qquad (1.7)$$

as $k \to \infty$, and where σ is a positive number. In addition, it is desirable to know that $\phi(u, k)$ is an analytic function of k in some sector $\{k\epsilon C: \left|\arg(k - k_o)\right| < d\}$. We can then compute $v(\kappa, \rho)$ via the Thiele algorithm, even though $\varepsilon(k, \kappa, \rho)$ may not be small over the range of values of k on which we know ϕ.

Now, if ϕ is known and can be evaluated for k on a finite interval, such as $I = \{k:k_{min} \leq k \leq k_{max}\}$, then we can apply the Thiele algorithm to the $2m + 1$ values

$$\rho_o^j \equiv \frac{\phi(u, k_j)}{a(k_j)}, \quad j = 0, 1, \ldots, 2m; \qquad (1.8)$$
$$k_j\epsilon I, \; k_j \text{ distinct.}$$

to accurately estimate $v(\kappa,\rho)$. The Thiele algorithm [2, 3, 4] involves using ρ_o^j defined in (1.8), and then computing the numbers

$$\rho_1^j = \frac{k_{j+1} - k_j}{\rho_o^{j+1} - \rho_o^j}, \quad j = 0, 1, \ldots, 2m - 1$$

$$\rho_i^j = \rho_{i-2}^{j+1} + \frac{k_{j+i} - k_j}{\rho_{i-1}^{j+1} - \rho_{i-1}^j}, \quad \begin{array}{l} j = 0, ., \ldots, 2m - i \\ i = 2, 3, \ldots, 2m. \end{array}$$
$$(1.9)$$

Some of these numbers can be used in a truncated continued fraction expansion of a rational function which interpolates the data ρ_o^j. That is, this rational function $R(k)$ is given by the continued fraction

$$R(k) = \rho_o^o + \frac{k - k_o}{\left|\rho_1^o\right.} + \frac{k - k_1}{\left|\rho_2^o - \rho_o^o\right.} + \ldots + \frac{k - k_{2m-1}}{\left|\rho_{2m}^o - \rho_{2m-2}^o\right.} \qquad (1.10)$$

and satisfies

$$R(k_j) = \rho_o^j, \; j = 0, 1, \ldots, 2m \qquad (1.11)$$

It is easy to see that the rational function (1.10) also has the form

$$R(k) = \frac{\rho_{2m}^o k^m + c_1 k^{m-1} + \ldots + c_m}{k^m + d1\, k^{m-1} + \ldots + d_m} \qquad (1.12)$$

where ρ_{2m}^o is the last entry computed in the table (1.9), and where c_i and d_i ($i = 1, 2, \ldots, m$) are the same constants. Hence, in addition to (1.11), $R(k)$ also satisfies the relation,

$$\lim_{k \to \infty} R(k) = \rho_{2m}^o \qquad (1.13)$$

i.e., we have the approximation,

$$v(\kappa,\rho) \cong \rho_{2m}^o. \qquad (1.14)$$

For example, for the case of the Helmholtz model (1.1), we have

$$\phi(u,k) \equiv \frac{1}{ik} \log u_k(\bar{r})\bigg|_{\bar{r}_s}^{\bar{r}_d} = \int_P \sqrt{1 + f(\bar{r})}ds + O(k^{-\sigma}),$$
$$k \to \infty$$
$$(1.15)$$

in which $v = \int_P \sqrt{1 + f}\,ds$, for the case of the Rytov approximation we have

$$\phi(u,k) \equiv \frac{2}{ik} w_k(\bar{r})\bigg|_{\bar{r}_s}^{\bar{r}_d} = \int_L f(\bar{r})ds + O(k^{-\sigma}), \; k \to \infty$$
$$(1.16)$$

where in (1.16), L is a straight line path joining $\bar{r}_s$ to $\bar{r}_d$ and $v = \int_L f\, ds$. The examples of this paper are based upon using (1.14) and (1.16). Eight significant figure accuracy is attainable, using $11(m = 5)$ or $13(m = 6)$ values for a 4 mm (FWHM) object with no of noise. However, the presence of noise diminishes this accuracy considerably, although it is possible to admit several powers of ten times as much noise via the use of ℓ_1 averaging.

If the influence of noisy data is not unduly destructive, we can use the above procedure to recover two functions $f(\kappa,\rho)$ and $g(\kappa,\rho)$ provided that $a(k)$ and $\delta > 0$ is known, and $\sigma > 0$ in the expression,

$$\phi(u,k) = a(k)\{f(\kappa,\rho) + k^{-\delta}[g(\kappa,\rho) + O(k^{-\sigma})]\}$$
$$(1.17)$$

In this case, we can recover $f(\kappa,\rho)$ by sampling

$$v = \frac{\phi(u,k)}{a(k)} \qquad (1.18)$$

Once $f(\kappa,\rho)$ has been determined via (1.14), we can apply the Thiele algorithm to

$$v = k^\delta\left[\frac{\phi(u,k)}{a(k)} - f(\kappa,\rho)\right] \qquad (1.19)$$

to get $g(\kappa,\rho)$.

2. ℓ_1 Averaging

In [1], ℓ_1 averaging was carried out <u>after</u>

application of the Thiele algorithm. We have since found that we can tolerate considerably more noise in the data by applying ℓ_1 averaging <u>before</u> application of the Thiele algorithm.

Since the data are complex numbers, actual ℓ_1 averaging is too difficult numerically. Instead, we carry out an ℓ_1 average on both the real and imaginary parts of the data separately. The process is very simple, and works as follows.

Given a set of real numbers $\{a_i\}_{i=1}^{M}$, we want to find a real number c^* which minimizes the sum

$$S(c) = \sum_{i=1}^{M} |a_i - c| \qquad (2.1)$$

The solution is

$$c^* = a_j \qquad (2.2)$$

where a_j is one of the values of $\{a_i\}_{i=1}^{M}$. Note that for even M, j may have two solution values. For odd M, c^* is the median, hence, the problem of finding c^* reduces to finding the minimum of the values

$$S(a_j) = \sum_{i=1}^{M} |a_i - a_j| \qquad (2.3)$$

with respect to j.

3. An Adaptive Feature

The method of ℓ_1 averaging provides a convenient procedure for adaptively choosing the number of terms in the rational function $R(k)$. For noisy data or for slowly changing ρ_i^j with respect to k_j, a better $R(k)$ is obtained by a rational function with a small number of terms.

In our test examples which follow, the method of ℓ_1 averaging was also applied to the odd rows ($i = 0, 2, 4, \ldots$) of the entries in the ρ table. For example, if all of the values of ρ^j in (1.8) are the same, there is no point in continuing, since this value is then also the limit as $k \to \infty$ of $R(k)$. Due to round-off error, the criterion actually used was to construct the ρ_{2i}^j entries of a particular row "2i", find the ℓ_1 average, c, with respect to j as described above, and then terminate the computations whenever the number of ρ_i^j (i fixed) such that $|\rho_i^j - c| \leq \delta$ was greater than the number of ρ_i^j such that $|\rho_i^j - c| > \delta$ for some small δ.

4. Numerical Experiments

We have tested the application of these methods with a series of computer simulations on the example illustrated in Fig. 1. This test case consisted of four objects with a distribution given by

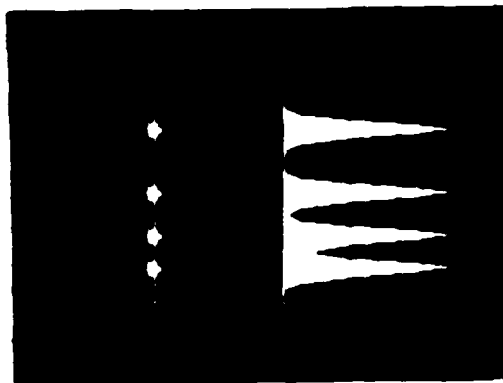$$f(\vec{r}) = e^{-b|\vec{r}-\vec{r}_j|^2} \qquad (4.1)$$

Fig. 1. Digitized image of test objects on a 41 x 41 grid with each pixel having dimensions of .3125 mm x .3125 mm. The FWHM for each of the Gaussian distributions is 1.0 mm and their centers are located at y = 3.75, 0.0, -2.5, and -4.375 mm. The bright line through the centers of these objects indicates the location of the data points for the intensity profile which is plotted on the right side.

where b was chosen so that the full width at half maximum of each object was 1 mm (which is 1.67 wavelengths at the central frequency of 2.5 MHz with the speed of sound c_0 = 1500 m/s) and the points r_i were chosen at x = 0 and y = 3.75, 0.0, -2.5, and -4.375 mm, respectively. All of the digitized images which we shall present for this test case will use a 41 x 41 grid with each pixel having dimensions .3125 mm x .3125 mm and with a profile of the brightened central line plotted to the right of the image.

The Rytov model was used to generate the forward scattering from these test objects. The line integrals of $f(\vec{r})$ can then be obtained from the asymptotic limit as $k \to \infty$ of (1.16); namely,

$$\lim_{k \to \infty} \frac{2}{ik} w_k(\vec{r}) = \int_L f(\vec{r}) \, ds \qquad (4.2)$$

where L is the straight line path from the source to our detector position. We use the Thiele procedure described in (1.8) to (1.14) to evaluate this asymptotic limit from an odd number of frequencies (usually 9 equi-spaced frequencies from 1 to 4 MHz).

These straight line integrals of $f(\vec{r})$ were calculated for a number (typically 55) of detector points spaced .3125 mm apart along a line oriented perpendicular to the direction of incident plane wave and located 8 cm from the x-y origin. Then, by taking data from multiple views (generally 30 views spaced 6° apart) and using ART, a well-known X-ray, computerized tomography algorithm, we were

able to reconstruct the distribution of $f(\vec{r})$. As we have shown in our previous paper [1], quite good reconstructions of $f(\vec{r})$ can be obtained provided we have very little noise in our data. An illustration of a reconstruction of $f(\vec{r})$ from reference [1] using random noise with a .1 percent standard deviation is given in Fig. 2. This re
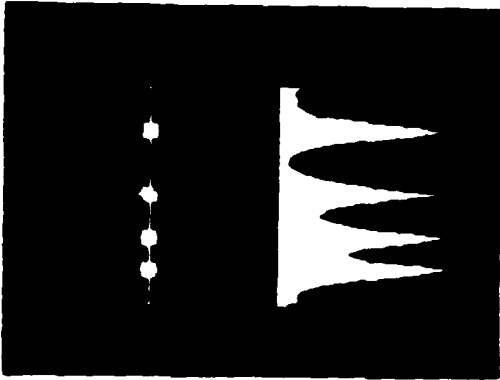

Fig. 2. Reconstruction of the test objects from 10 sets of 9 frequencies (uniformly spaced from 1-4 MHz) with .1 percent random noise using the ℓ-norm after applying the Thiele algorithm. Reprinted with permission from reference 1 (Stenger, F., et al., Proc. of Conf. on Wave Motion held at the University of Toronto, July, 1983, North Holland).

construction was obtained by using 10 distinct sets of 9 frequencies from 1-4 MHz and applying the ℓ-norm averaging to the results of the Thiele algorithm. However, the procedure of applying the ℓ_1 averaging after the Thiele procedure soon fails to produce acceptable results as we introduce increasingly larger amounts of noise, since the Thiele algorithm magnifies the noise. For example, Fig. 3 gives a reconstruction on data with 1.0 percent random noise using this method with 54 averages of each Thiele result. The objects are just barely recognizable and the peak values are low in magnitude by more than a factor of 2x.

Our new procedures described in sections 2 and 3 can readily handle noise of 1 or 2 percent. Figure 4 shows a reconstruction of our test case from data with 1 percent random noise using our new procedure with 54 averages. Although all of the objects are quite well resolved in Fig. 4, we discovered that by using a constraint condition in our reconstruction algorithm (based upon the fact that $f(\vec{r})$ was known to be of one sign), we were able to even further improve the resolution, as shown in Fig. 5 (notice the narrower line profiles and how much closer the troughs are to zero). Figure 6 shows how much more robust our new proce-
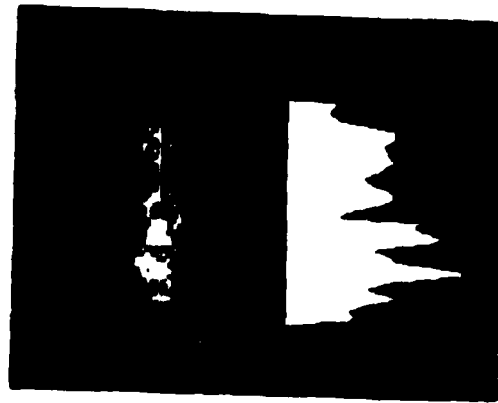

Fig. 3. Reconstruction of the test objects from data with 1 percent noise using the ℓ-norm procedure after applying the Thiele algorithm, as in the previous figure (but here the averaging was done with 54 repeats of noisy data using 9 equally spaced frequencies).
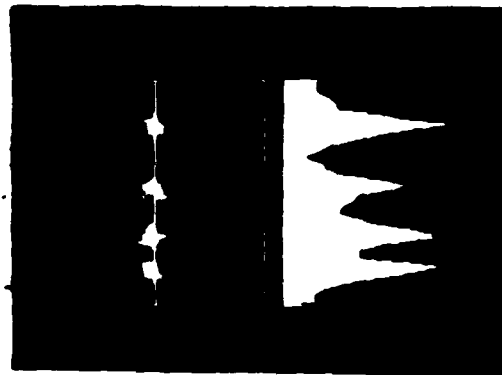

Fig. 4. Reconstruction of the test objects from data with 1 percent noise using our new ℓ_1 averaging and the adaptive feature described in sections 2 and 3. As in Fig. 3, the ℓ_1 averaging was obtained on 54 repeats on 9 equally spaced frequencies from 1-4 MHz.

dure is as this reconstruction was obtained from data with 1 percent noise using only 10 values in our ℓ_1 averaging. Using our previous method, we were not able to obtain recognizable images from only 10 ℓ_1 averages of data with 1 percent noise.

We also examined two other interesting questions. The first question concerned the applicability of using only the $\left(2v_k(\vec{r})/ik\right)$ term in
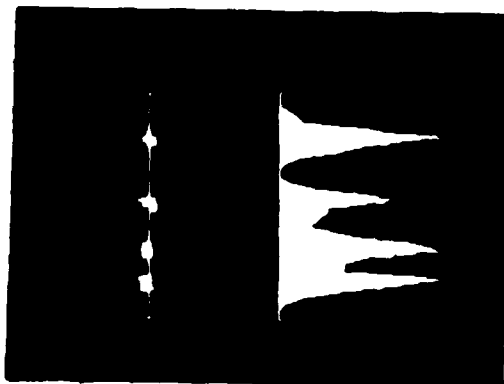
Fig. 5. Reconstruction of the test objects from
data with 1 percent noise obtained in the
same manner as Fig. 4., but using a con-
straint condition in ART based upon know-
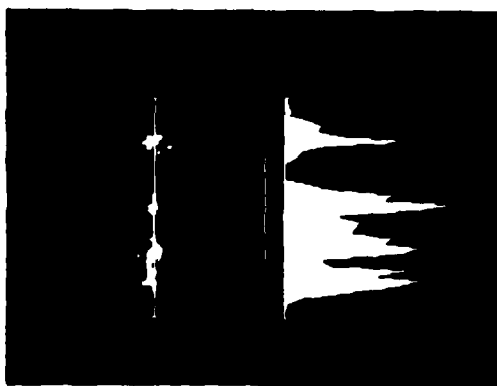ing that the distribution was of one
sign.

Fig. 6. Reconstruction of the test objects from
data with 1 percent noise using our new
procedure (as in Fig. 5), but doing the
ℓ_1 averaging over only 10 sets of data.
(For this reconstruction, a constraint
condition was also incorporated into the
ART algorithm which took advantage of the
knowledge that $f(\vec{r})$ was of one sign.)

(1.16) at a single wave number k as a first order
approximation to the asymptotic limit. We learned
that for the test object of Fig. 1 (FWHM = 2 mm),
this first term gives a completely unacceptable
approximation even without any noise. We could
not even distinguish the locations of the objects
if we used only this term.

The final question concerned the effect of
our stopping criteria. Our tests showed that
while the stopping procedure described in section
3 was quite helpful, it was not essential for ob-
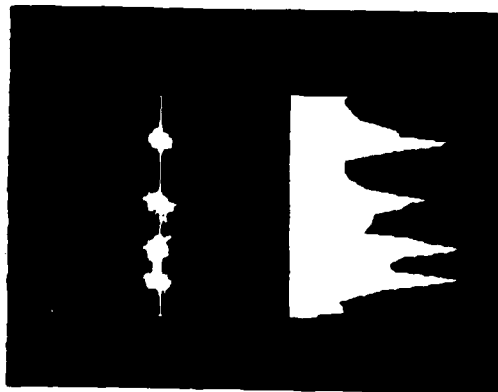taining a useable image. For example, Fig. 7

Fig. 7. Reconstruction of the test objects from
data with 1 percent noise. As for Fig.
3, we used the new ℓ_1 averaging procedure
on 54 sets of noisy data before applying
the Thiele algorithm, but here the stop-
ping criteria was omitted in the Thiele
procedure. Degradation from the results
in Fig. 4 where the stopping criteria was
used is apparent.

shows a reconstruction under the same basic situa-
tion as Fig. 4 (i.e., 9 frequencies using ℓ_1 aver-
aging 54 times before applying the Thiele proce-
dure), but without the stopping procedure. While
the resolution in 7 is much less than Fig. 4, one
can still clearly distinguish all four objects.

5. Conclusions

In a previous paper, we described the basic
idea of transforming the ultrasound inverse scat-
tering problem (with its attendant need to treat
diffraction effects in the measured scattering
data) to an equivalent X-ray CT-like problem (with
no diffraction effects in the new transformed
data) by the use of frequency extrapolation [3].
The basic idea of our method is to remove diffrac-
tion effects by generating a transformed projec-
tion of the object at infinite acoustic frequen-
cies [3]. Our early attempts to apply the method
met with limited success because of extreme sensi-
tivity to noise in the data. Applying ℓ_1 averag-
ing to many sets of frequency extrapolated projec-
tions helped improve noise tolerance, but probably
not enough for practical applications with real
data [1]. Our latest algorithm using ℓ_1 averaging
(median filtering) on the data before frequency
extrapolation combined with an adaptive frequency
extrapolation method provided even further im-
provements. Images have been made from simulated

data with 1 percent noise with as few as 10 sets of data combined by ℓ averaging. Such data could be obtained with existing tomographic scanners at frequencies below 4 MHz. Thus, our newest algorithm should now be tested with real scattering data to study its usefulness in ultrasound diffraction tomographic imaging. We also have shown in this paper how to reconstruct two material properties with differing dependencies on k. This suggests that our method might allow reconstruction of density in addition to speed of sound; however, this has not been verified.

Acknowledgments

References

1. Stenger, F., M. J. Berggren, S. A. Johnson, and C. H. Wilcox, "Rational Function Frequency Extrapolation in Ultrasonic Tomography," submitted to Proceedings of the Conference on Wave Motion, held at the University of Toronto, June 1983 (North Holland).

2. Ralston, A. and P. Rabinowitz, A First Course in Numerical Analysis, Problems 14-19, pp. 325-326 (McGraw-Hill, New York, 1978).

3. Stenger, F., "Asymptotic Ultrasound Inversion Based on Using More than One Frequency," in Acoustical Imaging 11, (Plenum Press, New York, 1981).

4. Stenger, F., "Explicit Nearly Optimal Linear Rational Rational Approximation with Preassigned Poles," submitted to Math Comp.

REPORT DOCUMENTATION PAGE		READ INSTRUCTIONS BEFORE COMPLETING FORM
1 REPORT NUMBER	2 GOVT ACCESSION NO AD·A136455	3 RECIPIENT'S CATALOG NUMBER
4 TITLE (and Subtitle) AN ADAPTIVE, NOISE TOLERANT, FREQUENCY EXTRAPOLATION ALGORITHM FOR DIFFRACTION CORRECTED ULTRASOUND TOMOGRAPHY		5 TYPE OF REPORT & PERIOD COVERED
		6 PERFORMING ORG. REPORT NUMBER
7 AUTHOR(s) F. Stenger M.J. Berggren S.A. Johnson		8 CONTRACT OR GRANT NUMBER(s) DAAG 29 83 K 0012
9 PERFORMING ORGANIZATION NAME AND ADDRESS Department of Mathematics Department of Bioengineering University of Utah, Salt Lake City, UT 84112		10 PROGRAM ELEMENT, PROJECT, TASK AREA & WORK UNIT NUMBERS
11 CONTROLLING OFFICE NAME AND ADDRESS U. S. Army Research Office Post Office Box 12211 Research Triangle Park, NC 27709		12 REPORT DATE Dec 1983
		13 NUMBER OF PAGES
14 MONITORING AGENCY NAME & ADDRESS(If different from Controlling Office)		15 SECURITY CLASS. (of this report) Unclassified
		15a DECLASSIFICATION DOWNGRADING SCHEDULE

16 DISTRIBUTION STATEMENT (of this Report)

Approved for public release; distribution unlimited.

17 DISTRIBUTION STATEMENT (of the abstract entered in Block 20, If different from Report)

NA

18 SUPPLEMENTARY NOTES

The view, opinions, and/or findings contained in this report are those of the author(s) and should not be construed as an official Department of the Army position, policy, or decision, unless so designated by other documentation.

19 KEY WORDS (Continue on reverse side if necessary and identify by block number)

20 ABSTRACT (Continue on reverse side if necessary and identify by block number)

In our previous work [1], a procedure was developed, based on algorithms for rational function frequency extrapolation and ℓ_1-norm averaging to circumvent both the effects of noise, and errors due to refracted curved paths, for solving the inverse scattering problem in ultrasonic imaging. In this paper, we reverse the order of the first two algorithms with respect to [1]; that is, we first apply the ℓ_1 averaging procedure and then carry out the rational function procedure, extrapolating to infinite frequency. An adaptive

method for choosing the best rational function expansion is also employed. We describe the underlying ideas of the procedure, and we illustrate examples of reconstructions in the presence and absence of Gaussian noise. These results are then compared with results of previous experiments. The resulting procedure works with a much smaller signal-to-noise ratio. An extension is suggested to image speed of sound and density.

84